

Electronic Supplementary Information (ESI)

Zambon A, Zoso A, Luni C, Frommer WB, Elvassore N. Determination of glucose metabolic fluxes in live myoblasts by microfluidic nanosensing and data analysis.

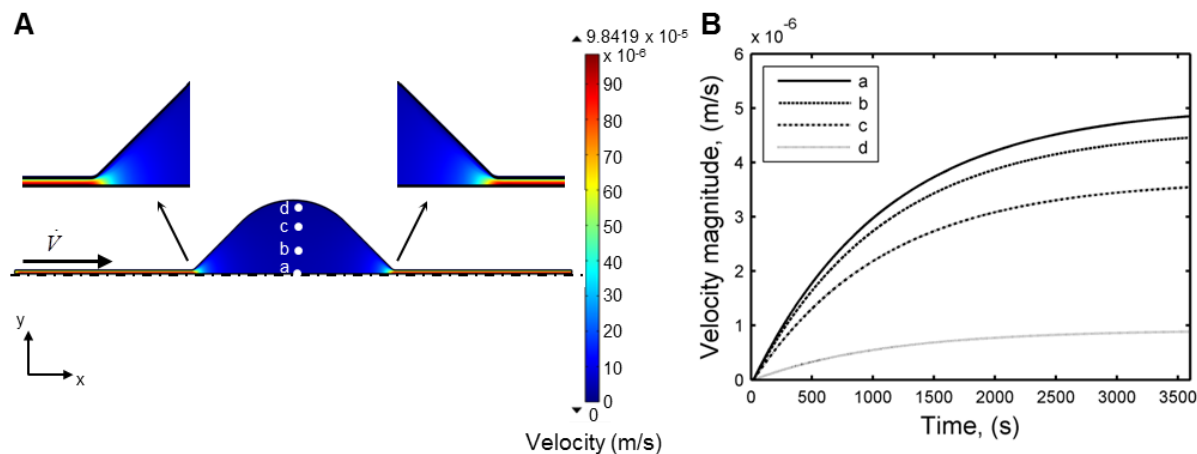


Figure S1. Fluid dynamics study using the developed 3D model. (A) Simulation of the velocity field at steady state in the median plane ($z = H/2$) of the culture chamber. Flow rate was $0.05 \mu\text{L}/\text{min}$. (B) Velocity magnitude during the step change in flow rate from 0 to $0.05 \mu\text{L}/\text{min}$. a, b, c, and d, refer to the positions indicated in A).

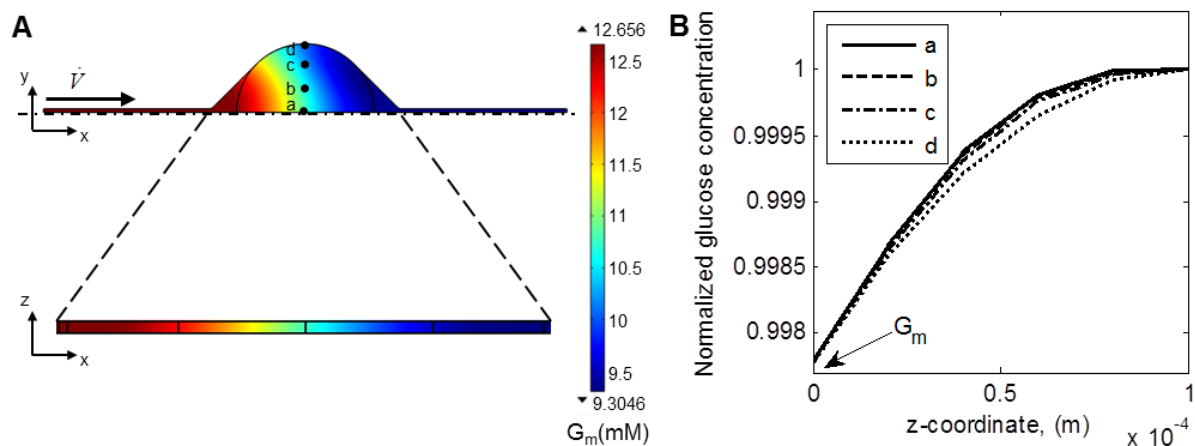


Figure S2. Study of the concentration profile within the microfluidic chip simulated by the developed 3D model. (A) Same as Figure 4C, with indicated the position of points a, b, c, d plotted in B). (B) Glucose concentration along the z-direction at positions indicated in A). Concentration was normalized by the concentration at the top of the channel ($z = H$) in each position.

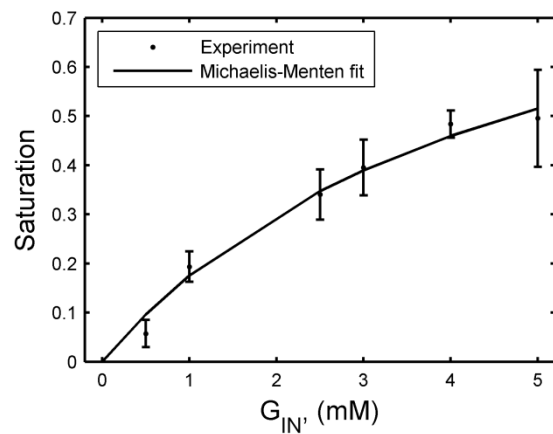
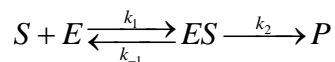


Figure S3. FRET-based nanosensor saturation curve. Saturation was calculated by Eq. (2) from the steady-state FRET data presented in Figure 5A. Solid line represents the results of least-square data fitting by a Michaelis-Menten-like equation.

Potential hexokinase enzymatic rate modification in the intra-cellular environment

We considered the classical elementary steps of an enzymatic reaction:



where S represents glucose, E hexokinase enzyme, ES the enzyme-substrate complex, and P glucose-6-phosphate. Mass-action kinetic parameters are indicated as k_1 , k_{-1} , and k_2 .

The Briggs-Haldane derivation of Michaelis-Menten equation assumes ES concentration is at quasi-steady state, i.e. in mathematical terms:

$$k_1 [E][S] \approx (k_{-1} + k_2)[ES] \quad (\text{S1})$$

where square brackets represent concentrations. Following this approximation the well-known Michaelis-Menten equation is obtained:

$$\frac{d[P]}{dt} = \frac{V_{\max} [S]}{K_m + [S]}, \quad (\text{S2})$$

where the values of parameters K_m and V_{\max} are related to the mass-action constants by the following expressions:

$$K_m = \frac{k_{-1} + k_2}{k_1}, \quad (\text{S3})$$

and

$$V_{\max} = k_2 [E]_0, \quad (\text{S4})$$

where $[E]_0$ is the total (constant) enzyme concentration in its bound and unbound states.

From Eqs. (S3) and (S4), the ratio of V_{\max} to K_m is given by the following relationship:

$$\frac{V_{\max}}{K_m} = \frac{k_2 [E]_0}{\frac{k_{-1} + k_2}{k_1}}. \quad (\text{S5})$$

Under the feasible assumption that $k_{-1} \ll k_2$, Eq. (S5) becomes:

$$\frac{V_{\max}}{K_m} \approx \frac{k_2 [E]_0}{\frac{k_2}{k_1}} = k_1 [E]_0. \quad (\text{S6})$$

Eq. (S6) shows that under the two simple assumptions above, it is possible to have a linear relationship between V_{\max} and K_m . Assuming that, compared to *in vitro* enzymatic experiments, the intra-cellular environment favors the production of glucose-6-phosphate by speeding up the reaction described by parameter k_2 , this would imply an increase in V_{\max} and K_m , without affecting their ratio.

Analysis of FRET-based nanosensor characteristic time

We performed further experiments using the FRET-based nanosensor to verify the accuracy of its time constant that we obtained. In particular, we stimulated the cells with approximately linear ramps of glucose concentration at increasing rate (Figure S4 A). According to the model developed, once the rise in glucose concentration is faster than the rate of nanosensor response, the nanosensor responds at its maximum rate and its half-time for saturation ($t_{1/2}$) is not affected by a further increase in the speed of the ramp any more (Figure S4 B).

The experimental results we obtained confirm this theoretical prediction. In particular, Figure S4 F shows that experimental results are in agreement with model simulations. Below about 10^0 min, the nanosensor characteristic time, the half-time for saturation remains approximately constant.

One would say that other resistances could be present that prevent nanosensor access to glucose as it is intracellular. However, we obtained the characteristic time of glucose uptake by myoblasts in culture, equal to 3.7 s, through repeated enzymatic assays of medium out flowing from the culture chamber, in a microfluidic culture system that enhanced the signal-to-noise-ratio. As the process of glucose transport through cell membrane is much faster than the interaction of glucose with the nanosensor, it is possible to analyze the kinetics of the nanosensor within the cell, because the cell membrane transport is essentially not affecting the measurement.

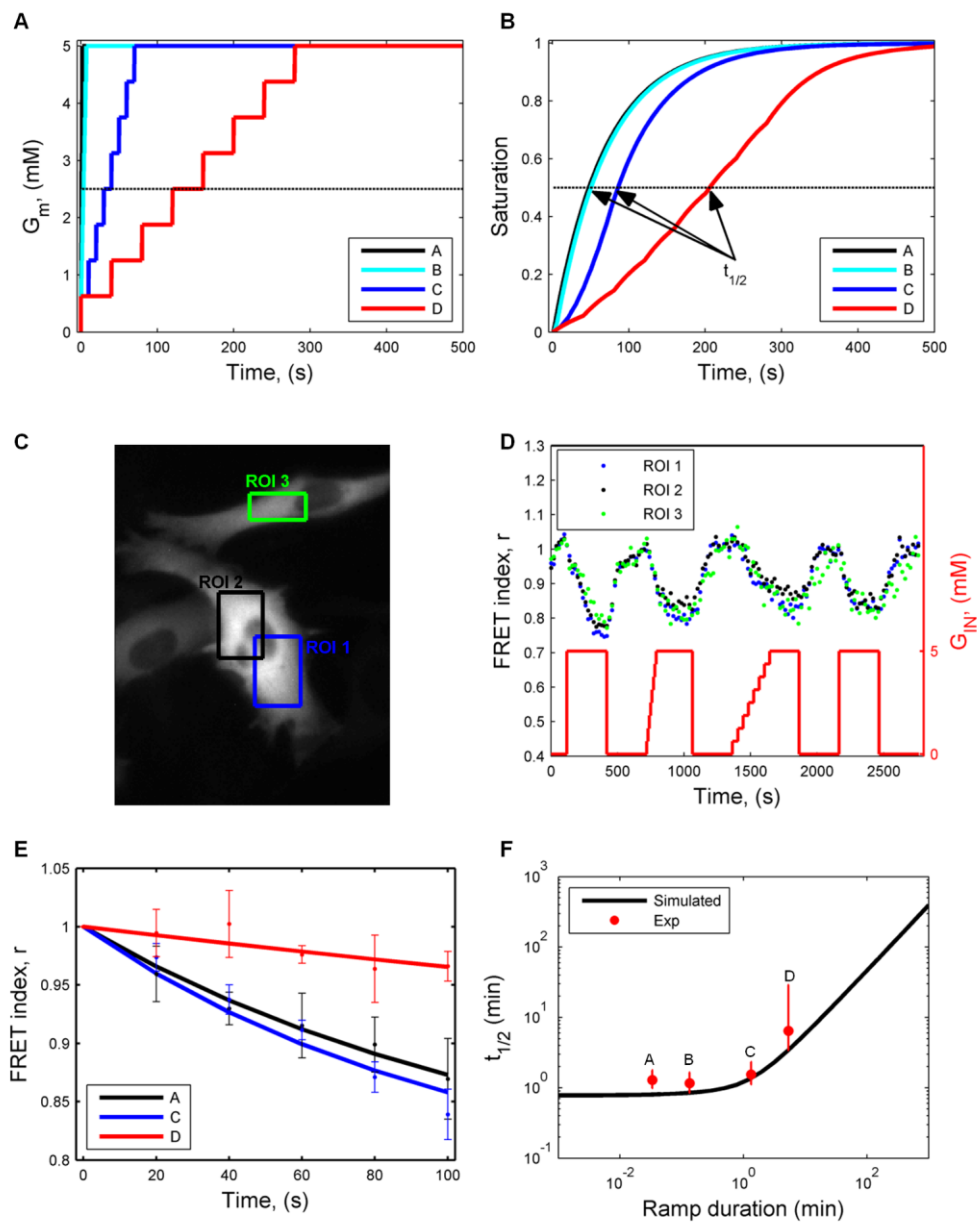


Figure S4. Study of FRET-based nanosensor time constant. (A) Simulated approximately linear ramps of glucose concentration of increasing rate. The step approximation mimics the inflow from the multi-inlet system into the culture chamber. (B) Model predictions of the nanosensor response to the stimuli described in (A). (C) Image of YFP fluorescence and indication of the ROIs analyzed in (D) and (E). (D) Experimental data of FRET-based nanosensor response to the glucose concentration profile indicated. (E) Analysis of the transient of FRET index decay following an increase in glucose concentration as shown in (D). Error bars indicate the standard deviation calculated from the 3 ROIs. (F) Comparison between the half-time for sensor saturation obtained by experimental data and model simulations. The experiment was repeated twice.

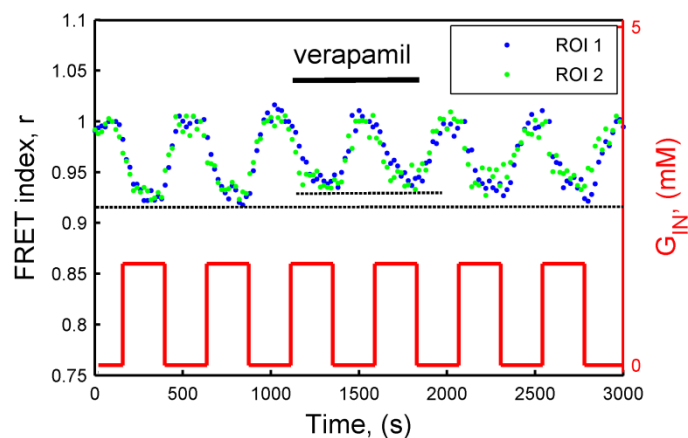


Figure S5. Effect of verapamil stimulation on cell response to glucose. Normalized baseline-corrected FRET index, r , as a function of time during repeated pulses of 1.5-mM glucose concentration, in presence or absence of glucose transport inhibitor, verapamil (150 μM). Removal of verapamil after 2 glucose pulses shows the inhibitory effect is reversible. Blue and green dots refer to the signal from 2 different cells. Flow rate was 4 $\mu\text{L}/\text{min}$.